16th World Conference on Earthquake, 16WCEE 2017

Santiago Chile, January 9th to 13th 2017

Paper N° 4057

Registration Code: S-E1463061883

ANALYTICAL SEISMIC FRAGILITY ANALYSIS OF BRIDGES EXCITED BY NEAR-FAULT PULSE-LIKE GROUND MOTIONS

D.G. Lu[(1)], Y. Liu[(2)], X. Yang[(3)]

[(1)] *Full professor, Harbin Institute of Technology, ludagang@hit.edu.cn*
[(2)] *PhD student, Harbin Institute of Technology, liuyang6886@163.com*
[(3)] *Graduate student, Harbin Institute of Technology, qdlgyx2008@126.com,*

Abstract

In this paper, based on the framework of the next generation performance-based earthquake engineering proposed by PEER, a method of simplified seismic fragility estimation has been developed for an illustrated bridge under near-fault earthquakes. First, the double-side pulse-like ground motion records are selected from the PEER NGA strong ground motion database based on the perk point method (PPM), and the far-field records are also selected following the opposite rules for comparison. To consider the characteristics of near-fault pulse-like ground motions, the spectral acceleration (S_a), the peak ground acceleration (*PGA*) and the peak ground velocity (*PGV*) are chosen as the intensity measures (*IM*s). With the aim at comprehensive investigation of multiple performance objectives, four engineering demand parameters (*EDP*s) for bridge components are defined, including the drift ratios of the middle pier and the side pier, the deformations of sliding bearings and fixed bearings. Based on a series of nonlinear dynamic time-history analysis of the case-study bridge using the OpenSees software, the probabilistic seismic demand models for each *EDP* and *IM* couples are established through regression analysis. Finally, the seismic fragility curves for bridge components and system are developed for different damage states. The numerical results highlight that the seismic demands of near-fault pulse-like ground motions are much larger than those of far-field ground motions, and that the middle pier is more fragile than side piers, and the failure probability of the system is larger than bridge components.

Keywords: bridge, near-fault pulse-like ground motion, probabilistic seismic demand model, seismic fragility, performance-based earthquake engineering

1. Introduction

A large number of earthquake damages indicate that near-fault pulse-like ground motions are different from far field ground motions, since this kind of ground motions contains large velocity pulses, which may induce heavy damage and lead to larger seismic demands for structures. As the important elements in transportation infrastructure, the collapse of bridges will directly lead to a lot of loss of lives and properties. As an important part of lifeline systems, the rescue work after disasters may be severely hampered. Therefore, the study on seismic response of bridges subjected to near-fault pulse-like ground motions and the development of seismic fragility curves of bridge components and systems is very important for transportation infrastructure safety and resilience under the environment of earthquakes.

The technique of fragility analysis has been widely used to estimate the seismic vulnerability of structures. During the traditional development of fragility curves, the probabilistic seismic demand analysis is a key element. For generation of the samples of earthquake events and structures, the Monte Carlo simulation approach is often used, which may cost lots of time. In fact, the uncertainty from seismicity is much larger than the uncertainty from structures. With the aim at focus on the seismic demand of the near-fault ground motions, the uncertainty from structures is neglected, and the cloud method for probabilistic seismic demand analysis is used in this paper.

In this paper, a typical RC continuous-girder bridge is taken as the case study, whose 3D finite element model is built on the OpenSees platform. To fully consider the uncertainties in the input seismic ground motions, 80 double-side pulse-like ground motion records are selected from the PEER NGA strong ground motion database based on the perk point method (PPM) [1]. For comparison, 80 far-field records are also selected following the opposite rules. Based on the responses of the bridge, the probabilistic demand analysis is performed. The seismic fragility curves of bridge components and systems subjected to near-fault pulse-like ground motions and far field ground motions are developed.

2. Selection and identification of ground motions

2.1 Selection of ground motions

A subset of ground motion records based on the PEER strong ground motion database of 80 near-fault (NF) pulse-like and 80 far-field (FF) are selected. The group of NF ground motion records is formed with the closest site-to-source distances (R) less than 20 km and the moment magnitudes (M_W) greater than 6.0. The ratio of PGV and PGA is greater than 0.2 for making sure that the ground motions include obvious velocity pulse. Through direct observation, the ground motions records in the NF group should have double side velocity pulses. On the rule of R > 20 km, the FF ground motion records are selected to match the PGA and M_w of the NF records, which are compatible with the values of PGA and M_W of the NF records. The M_w -PGA data are shown in Fig. 1.

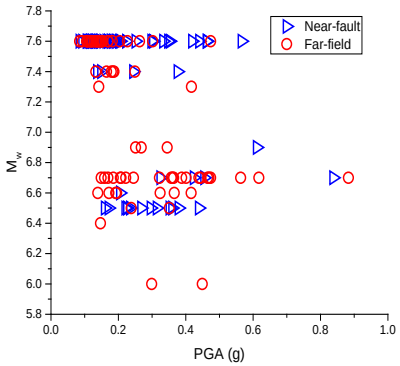

Fig. 1 – M_w-PGA data of ground motions

The 80 NF ground motions records come from 5 strong earthquakes. These strong shock earthquakes are N. Palm Springs Earthquake (America, 1986), Imperial Valley Earthquake (America, 1979), ChiChi Earthquake (Taiwan, 1999), Kocaeli Earthquake (Turkey, 1999) and Northridge Earthquake (America, 1994). 80 FF ground

motions records from 7 strong shock earthquakes are also selected, which are the same as the NF and the Kobe Earthquake (Japan, 1995), Whittier Narrows Earthquake (America, 1987). Due to limited space, the list of the selected ground motions is not listed, but the response spectrum of NF pulse-like ground motions are shown in Fig. 2.

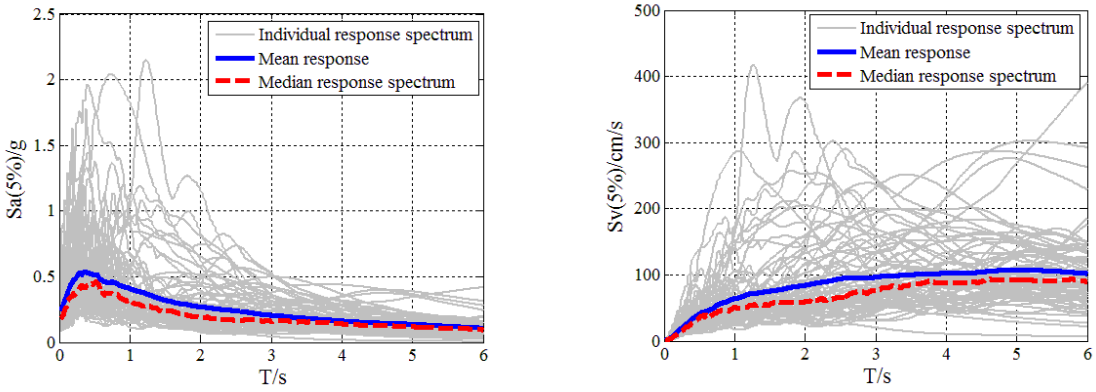

(a) Acceleration response spectrum (b) Velocity response spectrum

Fig. 2 – Response spectrum of near-fault pulse-like ground motions

2.2 Identification of velocity pulses

In this paper, an approach based on energy to quantitatively identify the NF pulse-like ground motions is used.

First, the real ground motion time-histories are matched to the simplified mathematical pulse model by the least square method. Then, the simplified time-histories with characteristics of main pulse are got. Second, the perk-point method (PPM) is used to identify the parameters (period of pulse, perk velocity) of the main pulses of real ground motions. Finally, the energy index Ep is defined to identify the pulse-like ground motion.

The pulse model [2] is defined as

$$v_p(t;V_p,T_p,N_c,T_{pk},\varphi)=V_p\exp\left[-\frac{\pi^2}{4}\left(\frac{t-T_{pk}}{N_cT_p}\right)^2\right]\times\cos\left(2\pi\frac{t-T_{pk}}{T_p}-\varphi\right) \quad (1)$$

in which, v_p is the extracted velocity pulse, V_p is pulse amplitude, T_p is period of pulse, N_c is the number of cycles in the pulse, T_{pk} is the location of the pulse. Through the least square method, the velocity pulse in real ground motion time-histories are matched with the simplified mathematical model. Based on the velocity pulse model from the real ground motion, the PPM [3] is used to define the time interval of valley and peak in time-history curves as the pulse period. The pulse period results of the 80 near-fault ground motions records are identified.

To identify the velocity pulse ground motion, the energy index E_p is defined as

$$\begin{cases} E(t)=\dfrac{\int_0^t v^2(\tau)d\tau}{\int_0^\infty v^2(\tau)d\tau} \\ E_p=\int_{t_s}^{t_e}dE(t)=E(t_e)-E(t_s) \end{cases} \quad (2)$$

in which, $E(t)$ is cumulative energy of a ground motion at time t; $v(\tau)$ is the velocity time series; t_s and t_e represent the starting and ending time points of a velocity pulse. The range of E_p calculated is 032 to 0.89. When

the E_p is greater than 0.3, the NF ground motion records include obvious velocity pulses [4]. According to the energy index results, all the selection NF ground motion records include obvious velocity pulses.

3. Description of the case study and FE model

3.1 Description of the case study

The case study is illustrated by a typical 4-spans reinforced concrete (RC) continuous girder bridge which is designed according to the Chinese seismic design code [5]. The straight bridge is 72.0 m long and consists of four spans of 18.0 m. The total width of the road cross-section is 8.9 m, with carriageway 7.5 m wide without sidewalks. This is a typical overpass cross-section with 2 traffic lanes. The cross section of the main beam has a single-box single-room section with the total height of 1.5 m (Fig. 3). The thickness of the top concrete slab is equal to 25 cm. The box beam is simply supported on normal (low-damping) damping rubber bearings at the intermediate pier. At the abutments, the sliding bearings are used. The column type pier is 7.0 m height with the diameter of 1.5 m, while 32 mm of diameter of 25 reinforcement bars along the longitude direction.

The grade of concrete for the superstructure is C40 with the thickness of concrete cover 5 cm, while the C30 grade concrete are used for piers and abutments. The reinforcement bars are made of grade HRB335 steel. It is assumed that the foundation soil is categorized as type C and the soil-structure interaction (SSI) effect is neglected in this case.

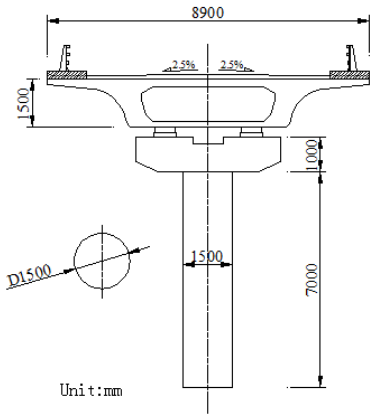

Fig. 3 – Cross section at pier for selected bridge

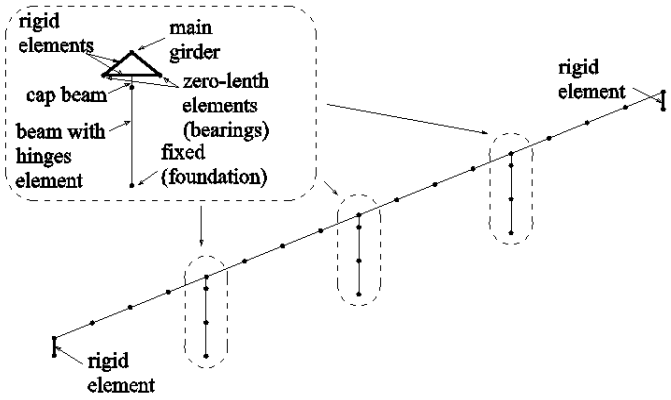

Fig. 4 – 3-D finite element model of the bridge

3.2 Finite element model

In this case of the RC continuous bridge, the 3D finite element (FE) model is built on the OpenSees platform (Fig.3) [5]. In the FE model, the nonlinearity of materials is considered. The concrete01 type is selected as the mechanical model of concrete according to the Kent-Scott-Park model where the tensile strength of concrete is neglected, with the Poisson's ratio of concrete 0.2, Young's modulus E = 30000 MPa and 32500 MPa. Meanwhile, the steel01 type, an elastic-perfectly plastic model, is selected as the mechanical model of steel bars assuming that the tensile properties is as the same as the properties of compression. The young's modulus of steel is 200000 MPa.

The typical RC box beam is modeled using linear elastic beam elements. Since the superstructure is not expected to yield [6], the simplified modeling solution described above is preferred to drastically reduce the computational cost of the numerous time history analyses performed for this study [7]. For the reinforced concrete piers, the nonlinear beam elements with fiber section are used to simulate the nonlinear behavior of piers. The SSI effect is neglected with piers fixed on the earth. In this case, the abutments are neglected and the supports at the end of beams are simulated by sliding bearings.

The bearings are simulated by zero-length elements which are similar to springs with different stiffness. According to many tests of dynamic behavior, the hysteretic curves of the plate rubber bearings are narrow shape, where they can be similarly described as linear behavior. In this FE model, the longitude stiffness of the plate rubber bearings are calculated according to guidelines for seismic design of highway bridges [6]:

$$K_H = \frac{A_R G}{\sum t_e} \tag{3}$$

where A_R = shear area of bearing, Σt_e = total thickness of rubber layers, G = shear modulus of rubber layer. The dynamic behavior of the polytetrafluoroethylene (PTFE) slide plate bearings is simulated by the elastic-perfectly plastic material, whose stiffness before sliding can be calculate as the same as the plate rubber bearings. The critical displacement of sliding is defined as

$$x_y = \frac{F_{\max}}{K} = \frac{f \cdot N}{K} \tag{4}$$

where $F_{\max}$ is the critical friction force, K is the initial stiffness, the coefficient of sliding friction f = 0.05, N is the dead load carried by the bearings.

4. Probabilistic seismic demand analysis

4.1 Definitions of intensity measures and engineering demand parameters

A lot of intensity measures (IMs) can be selected for probabilistic seismic demand analysis (PSDA), however, selection of the optimal IM for the probabilistic seismic demand model (PSDM), which considers the uncertainty of ground motions, would need a lot of work. As shown in Table 1, 6 intensity measures are selected in this paper.

Table 1 – Intensity measures selected

No.	*IM*	Definition	Unit
1	Peak ground acceleration	$PGA = \max\left\|\ddot{u}_g(t)\right\|$	g
2	Spectral acceleration	$S_a(T,\xi)$ for damping ratio ξ at period T	g
3	Peak ground velocity	$PGV = \max\left\|\dot{u}_g(t)\right\|$	cm/sec
4	Velocity pulse period	The Period of velocity pulse	sec
5	Maximum Increment Velocity	$MIV = \max(\int_0^T \left\|\ddot{u}_g(t)\right\| dt)$	cm/sec
6	Maximum Increment Displacement	$MID = \max(\int_0^T \left\|\dot{u}_g(t)\right\| dt)$	cm

The different engineering demand parameters (EDPs) can represent different performance of bridges, which can be classified as global, intermediate and local level groups, also can be sorted to different component groups. In this study, the relative maximum displacement ductility of piers (μ_d) is selected as the pier EDP, defined as

$$\mu_d = \frac{\Delta}{\Delta_{cy1}} \tag{5}$$

where, Δ is the maximum horizontal relative displacement between the top node and bottom node of piers, Δ_{cy1} is the relative displacement when the longitude bars begin to yield, it describes the overall bridge behavior under seismic loading [8]. The maximum deformation of bearings (D) is also selected as the EDP to describe the performance of bearings.

4.2 Probabilistic seismic demand models

Based on the 160 samples of ground motion – structures, the seismic responses of the structure are got by nonlinear dynamic time-history analysis. The total of 160 nonlinear analysis data provides the parameters of the conditional probability distribution of the *EDP* given *IM*. Assuming that the *EDP* has a lognormal distribution, the conditional mean of *EDP* given *IM* can be assumed linear in the log-log space, whereas the conditional dispersion is assumed as a constant. Thus, the probabilistic seismic demand model (PSDM) can be expressed as

$$\ln(\overline{EDP}) = a + b\ln(IM) \tag{6}$$

in which, a and b are regression parameters. The logarithmic standard deviation could be obtained as following:

$$\beta_{EDP|IM} = \sqrt{\frac{\sum_{i=1}^{N}\left(\ln\left(EDP_i\right) - \ln\left(\overline{EDP}\right)\right)^2}{N-2}} \tag{7}$$

where, N is the number of fitting data.

Through significance test of regression coefficients of the demand model, the logarithmic standard deviation $\beta_{EDP|IM}$ and the coefficient of determination R^2 can be used to test the efficiency of the selected intensity measures. For the near-fault ground motions, the T_p, *MIV* and *MID* cannot completely pass the test, so only the *PGA*, *PGV* and S_a are selected as the optimal intensity measures. The test results are shown in Fig. 5. It can be found that S_a has the strongest dependency with the responses of the bridge.

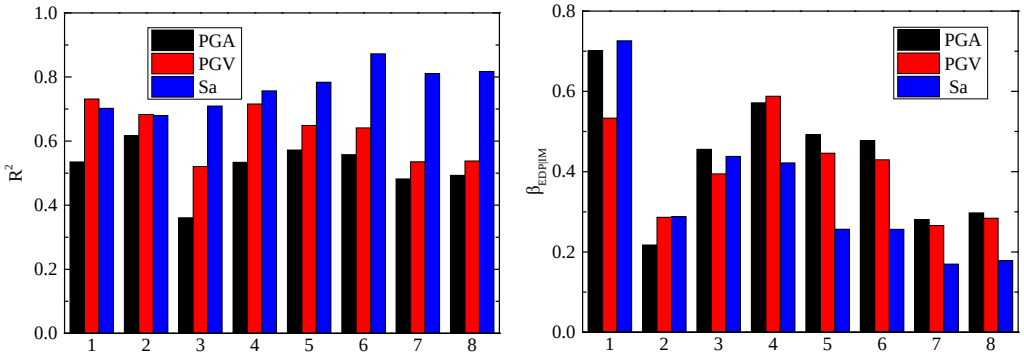

(a) Near-fault ground motions

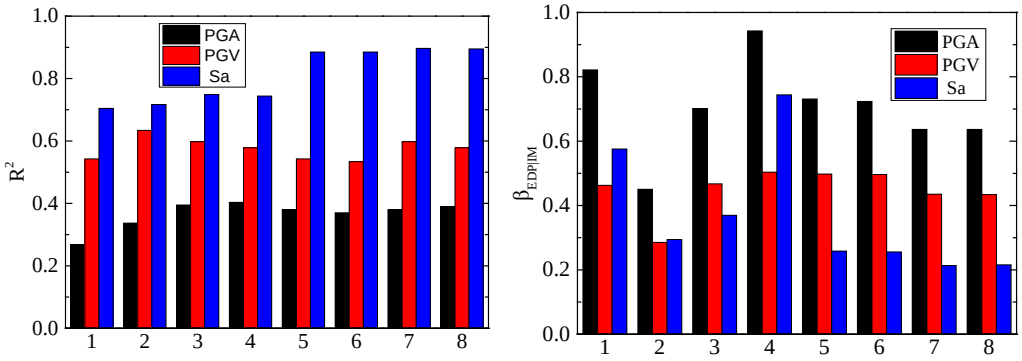

(b) Far-field ground motions

Fig. 5 – Results of significance testing of regresssion coefficients

The results of the demand analysis with *IM* being *PGA*, *PGV* and S_a for longitudinal direction excitation are shown in Table 2, while the results for transverse direction excitation are shown in Table3.

We can find that the goodness of fit for demand models with S_a being *IM* is better than other models with *PGV* and *PGA* at transverse direction. While the goodness of fit for demand models with *PGA* is the lowest even for FF ground motions, the reason is that the horizon of *PGA* selected is limited. As shown in Table 2, the *PGV* and S_a exhibited the better goodness of fit than *PGA*, while for side piers and sliding bearings the goodness of fit with *PGV* is even better. The reason is due to the settlement of the sliding bearings settled at side piers. According to the regression results for the majority, the goodness of fit for FF ground motions is better than NF ground motions. This may be due to the more uncertainty in NF ground motions. In general, S_a exhibits more dependence with responses of the structure than *PGV* for both NF ground motions and FF ground motions.

Table 2 – Results of demand analysis for longitudinal direction shocking

Component	Intensity measures	*a*		*b*		$B_{EDP\|IM}$		R^2	
		NFGM	FFGM	NFGM	FFGM	NFGM	FFGM	NFGM	FFGM
Middle pier	PGA	2.96	-0.67	1.45	0.42	0.7	0.82	0.54	0.27
	PGV	-7.22	-4.86	1.93	1.23	0.53	0.46	0.70	0.54
	Sa	2.06	0.29	1.22	0.92	0.73	0.58	0.73	0.70
Side pier	PGA	-1.38	-1.81	0.42	0.29	0.22	0.45	0.78	0.34
	PGV	-1.67	-3.55	0.34	0.45	0.29	0.29	0.68	0.73
	Sa	-3.86	-1.75	0.44	0.29	0.29	0.29	0.68	0.72
Fixed bearing	PGA	4.72	3.75	0.32	0.43	0.46	0.7	0.36	0.39
	PGV	2.45	-0.13	0.43	1.12	0.39	0.47	0.52	0.6
	Sa	4.56	4.53	0.29	0.82	0.44	0.37	0.71	0.75
Sliding bearing	PGA	7.35	4.64	1.18	0.61	0.57	0.94	0.53	0.4
	PGV	-0.99	-0.58	1.59	1.48	0.59	0.5	0.75	0.58
	Sa	6.63	5.64	1.00	1.11	0.42	0.74	0.71	0.74

*NFGM: near-fault ground motions; FFGM: far-field ground motions;

Table 3 – Results of demand analysis for transverse direction shocking

Component	Intensity measures	*a*		*b*		$B_{EDP\|IM}$		R^2	
		NFGM	FFGM	NFGM	FFGM	NFGM	FFGM	NFGM	FFGM
Middle pier	PGA	1.55	-0.42	1.09	0.4	0.49	0.73	0.57	0.08
	PGV	-5.62	-4.3	1.33	1.13	0.45	0.5	0.65	0.57
	Sa	1.17	0.58	1.19	0.93	0.26	0.26	0.88	0.88
Side pier	PGA	1.22	-0.67	1.03	0.38	0.48	0.72	0.56	0.07
	PGV	-5.56	-4.42	1.26	1.1	0.43	0.5	0.64	0.56
	Sa	0.87	0.35	1.12	0.91	0.26	0.26	0.87	0.88
Fixed bearing	PGA	5.01	4.11	0.52	0.36	0.28	0.64	0.48	0.08
	PGV	1.63	0.72	0.63	0.98	0.27	0.44	0.54	0.57
	Sa	4.86	4.97	0.59	0.81	0.17	0.21	0.81	0.9
Sliding bearing	PGA	4.89	3.9	0.56	0.37	0.3	0.64	0.49	0.09
	PGV	1.25	0.48	0.67	0.99	0.28	0.43	0.54	0.57
	Sa	4.71	4.75	0.63	0.81	0.18	0.22	0.82	0.89

*NFGM: near-fault ground motions; FFGM: far-field ground motions;

5. Seismic fragility analysis

5.1 Definition of damage measures

The whole bridge is supported by piers and abutments. The piers often firstly begin to be damaged under a strong motion shocking. The column failure can result in a series of disasters. In this paper, the displacement ductility of piers is defined as the damage measure. According to Hwang's research report, five damage states [9] are defined by displacement ductility [10]. With the aim at getting the damage index (DI), the moment-curvature analysis with the RC section is performed [11]. The damage indices of piers are shown in Table 4.

Table 4 – Damage states and damage indices

Damage state	DIs for pier	DIs for fixed bearing (mm)	DIs for sliding bearing (mm)
no damage	$\mu_d \le 1$	$D \le 30$	$D \le 50$
slight	$1 < \mu_d \le 1.07$	$30 < D \le 50$	$50 < D \le 100$
moderate	$1.07 < \mu_d \le 1.31$	$50 < D \le 100$	$100 < D \le 150$
extensive	$1.31 < \mu_d \le 4.31$	$100 < D \le 255$	$150 < D \le 300$
complete	$\mu_d > 4.31$	$D > 255$	$D > 300$

Bearings generally are the most vulnerable components for RC continuous-girder bridges. Some slight damage of superstructures occurs, while the bearings are extensively damaged. The displacement D of bearings is selected as the damage measure for bearings. According to Nielson's research work [12], the DIs for bearings are also shown in Table 4.

5.2 Seismic fragility functions

Assuming that the seismic demand of structures and the DM all follow lognormal distributions, the conditional failure probability P_f given the IM, which represents the probability of the seismic damage exceeding the certain damage indices, can be defined as

$$P_f = \Phi\left[\frac{-\ln\left(DI_i / m_{EDP}\right)}{\sqrt{\beta_{DM}{}^2 + \beta_{EDP|IM}{}^2}}\right] \tag{8}$$

where, the DI_i can be selected from Table4, β_{DM} is the logarithmic standard deviation of DM assumed as 0.2, $\beta_{EDP|IM}$ is the despersion of the seismic demand, which can be gotten from Table 2 and Table 3. The median of demand m_{EDP} can be calculated by regression analysis of seismic demand analysis data.

The fragility curves of bridge components with the input parameter S_a are illustrated in Fig.5 and Fig.6. Fig. 6 shows the fragility curves of bridge components under the longitudinal seismic loading. It can be found that the exceedance probabilities of slight and moderate damage for bearings are greater than those for piers, but the exceedance probabilities of extensive and complete damage are smaller than those for piers. The exceedance probabilities of slight and moderate damage for fixed bearings are larger than those for sliding bearings, whereas there is a revere situation for heavy damage. There is a similar situation for middle piers and side piers. The probability of slight and moderate damage for middle piers is greater than side piers. It can be concluded that, when the bridge is excited by longitudinal earthquakes, the fixed bearing at the middle pier is firstly damaged, and then the sliding bearings at abutments will start to be damaged. After that, the piers will exhibit the slight damage until the heavy damage situation appears. Finally, the bearings will be destroyed subsequently. That is because the difference of stiffness of components distribution, and the most rigid component will start to exhibit the damage in advance, and will be the last one completely destroyed. For all the damage states, the exceedance

probability under NF ground motions is greater than FF ground motions.

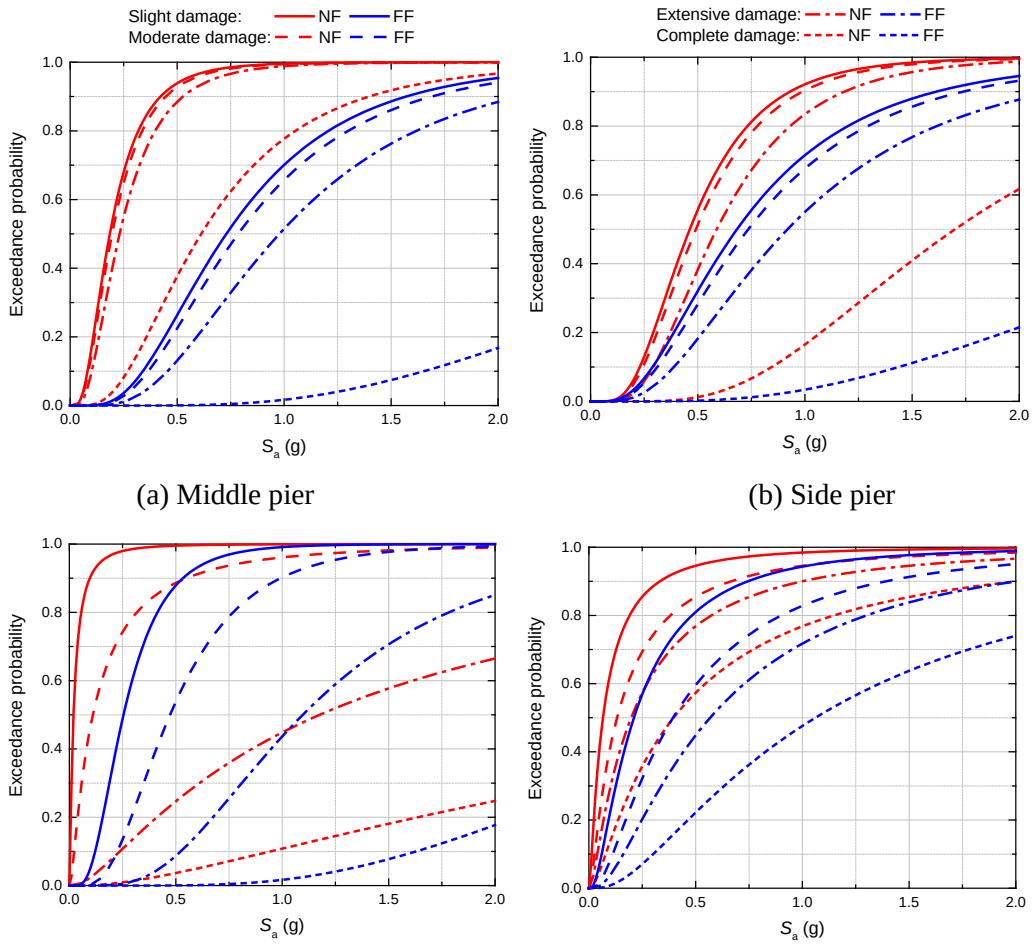

(a) Middle pier (b) Side pier

(c) Fixed bearing (d) Sliding bearing

Fig. 6 – Fragility curves of componets for longitudinal direction ground motions

The fragility curves of components under transverse loading (Fig. 7) show the similar results to Fig. 6. However, the exceedance probability of damage for components at this direction is smaller than the longitudinal direction. That is because the movement in transverse direction is limited in the FE models, but the failure probability under the near-fault ground motions shocking is also greater than the far-field ground motions.

The bridge system fragility curves are more useful when the decisions with assessment and reinforcement are made. Based on the component fragility curves, the system fragility curves can be easily derived. Assuming that the components of the bridge are mutually independent, the bridge can be modeled as a series system:

$$P_{fs} = 1 - \prod_{i=1}^{n} \left[1 - P_{fi} \right] \tag{9}$$

in which, P_{fs} is the system failure probability, P_{fi} is the failure probability of component i.

The fragility curves of the bridge system can be calculated according to Eq. (9), the results are shown in Fig. 8. Comparing the fragility curves of bridge system and the components, I can be seen that the damage probability of the system is greater than the components. For the system fragility, the damage probability of the bridge shocked in the longitude direction is larger than the transverse direction. It is worth mentioning that the failure probability of the bridge system for near-fault ground motions is always greater than the far-field ground motions.

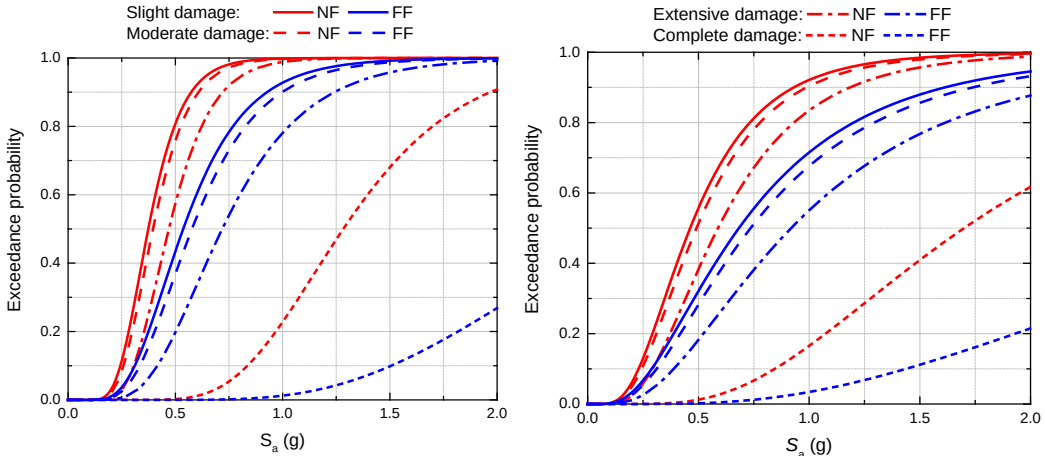

(a) Middle pier (b) Side pier

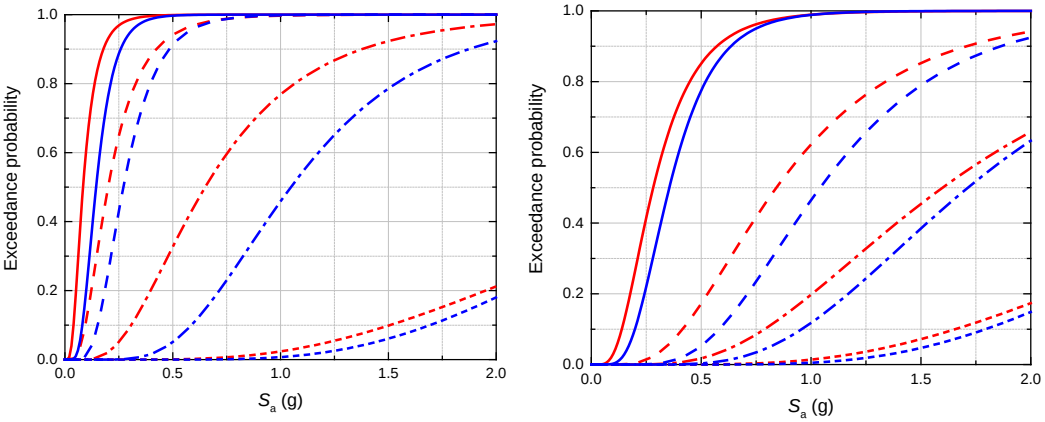

(c) Fixed bearing (d) Sliding bearing

Fig. 7 – Fragility curves of bridge components for transverse direction ground motions

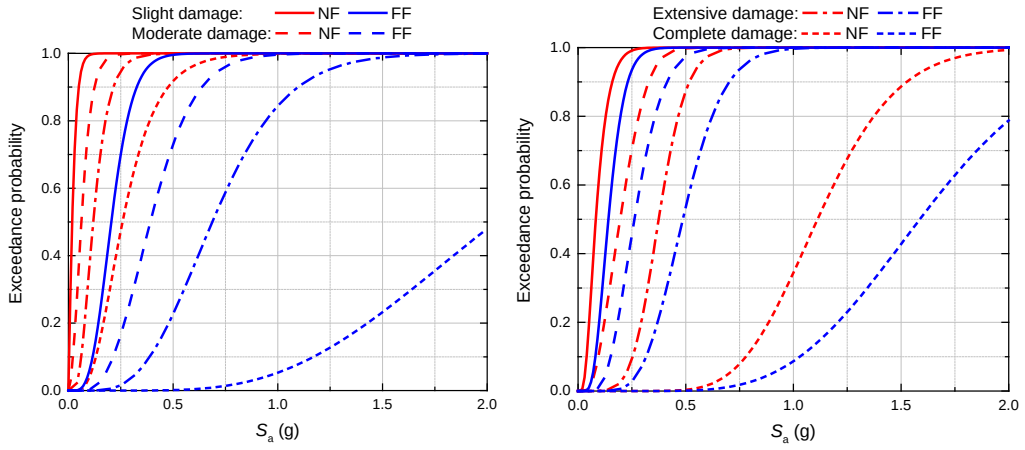

(a) Longitudinal direction (b) Transverse direction

Fig. 8 – Fragility curves of the system

6. Conclusions

Through seismic fragility analysis of the case-study bridge, the following conclusions can be obtained:

(1) The fragility of the bridge under the near-fault pulse-like ground motions is larger than that under the far-field ground motions.

(2) The spectral acceleration S_a exhibits more goodness of fit than the peak ground velocity *PGV* and the peak ground acceleration *PGA* for the probability seismic demand models.

(3) The fixed bearing is the most fragile component in this case, while the middle piers are more vulnerable than side piers. The seismic fragility of the system is larger than that of bridge components.

8. Acknowledgements

The financial supports received from the National Science Foundation of China (Grant Nos. 91315301, 51378162, 51178150), the Research Fund from Ministry of Science and Technology of China (2013BAJ08B01), and the Open Research Fund of State Key Laboratory for Disaster Reduction in Civil Engineering (SLDRCE12-MB-04) are gratefully appreciated.

9. References

[1] Baker JW (2007): Quantitative classification of near-fault ground motions with wavelet analysis. *Bulletin of the Seismological Society of America*, 97(5), 1486-1501.

[2] Dickinson BW, Gavin HP (2011): Parametric statistical generalization of uniform hazard earthquake ground motions. *Journal of Structural Engineering*, ASCE, 137(3), 410-422.

[3] Osaki Y (2008): *Spectral Analysis in Earthquake Engineering*, Beijing: Seismological Press.

[4] Zhai C, Chang Z, Li S, Chen ZQ, Xie L (2013): Quantitative Identification of Near-Fault Pulse-Like Ground Motions Based on Energy. *Bulletin of the Seismological Society of America*, 103(5), 2591-2603.

[5] McKenna F, Mazzoni S, Scott MH, Fenves GL (2007): *OpenSees command language manual*. Pacific Earthquake Engineering Research Center, University of California, Berkeley.

[6] JTG /TB 01-2008 (2008): *Guidelines for seismic design of highway bridges*.

[7] Tubaldi E, Barbato M, Dall'Asta A (2010): Transverse seismic response of continuous steel-concrete composite bridges exhibiting dual load path. *Earthquakes & Structures*, 1(1), 21-41.

[8] Tondini N, Stojadinovic B (2012): Probabilistic seismic demand model for curved reinforced concrete bridges. *Bulletin of Earthquake Engineering*, 10(5), 1455-1479.

[9] Park YJ, Ang AHS (1985): Mechanistic Seismic Damage Model for Reinforced Concrete. *Journal of Structural Engineering*, ASCE, Vol. III, No. 4, 722-739.

[10] Hwang H, Liu JB, Chiu YH (2001): Seismic Fragility Analysis of Highway Bridges. *Mid-America Earthquake Center Technical Report*, MAEC-RR-4 Project.

[11] Lu DG, Liu Y, Yu XH, Huang MG (2015): Probabilistic seismic demand models and fragility analysis of RC continuous girder bridges, *Symposium on Reliability of Engineering System* (*SRES'2015*), China.

[12] Nielson BG (2005): Analytical Fragility Curves for Highway Bridges in Moderate Seismic Zones. *Ph.D. Dissertation*, Georgia Institute of Technology.